PHYSICAL REVIEW C **86**, 051301(R) (2012)

Shape transitions in exotic Si and S isotopes and tensor-force-driven Jahn-Teller effect

Yutaka Utsuno,[1,2] Takaharu Otsuka,[2,3,4,5] B. Alex Brown,[4,5] Michio Honma,[6] Takahiro Mizusaki,[7] and Noritaka Shimizu[2]

[1]*Advanced Science Research Center, Japan Atomic Energy Agency, Tokai, Ibaraki 319-1195, Japan*

[2]*Center for Nuclear Study, University of Tokyo, Hongo, Bunkyo-ku, Tokyo 113-0033, Japan*

[3]*Department of Physics, University of Tokyo, Hongo, Bunkyo-ku, Tokyo 113-0033, Japan*

[4]*National Superconducting Cyclotron Laboratory, Michigan State University, East Lansing, Michigan 48824, USA*

[5]*Department of Physics and Astronomy, Michigan State University, East Lansing, Michigan 48824, USA*

[6]*Center for Mathematical Sciences, University of Aizu, Ikki-machi, Aizu-Wakamatsu, Fukushima 965-8580, Japan*

[7]*Institute for Natural Sciences, Senshu University, Tokyo 101-8425, Japan*

(Received 23 August 2012; published 8 November 2012)

We show how shape transitions in the neutron-rich exotic Si and S isotopes occur in terms of shell-model calculations with a newly constructed Hamiltonian based on $V_{\rm MU}$ interaction. We first compare the calculated spectroscopic-strength distributions for the proton $0d_{5/2,3/2}$ and $1s_{1/2}$ orbitals with results extracted from a ^{48}Ca$(e,e'p)$ experiment to show the importance of the tensor-force component of the Hamiltonian. Detailed calculations for the excitation energies, $B(E2)$, and two-neutron separation energies for the Si and S isotopes show excellent agreement with experimental data. The potential-energy surface exhibits rapid shape transitions along the isotopic chains towards $N = 28$ that are different for Si and S. We explain the results in terms of an intuitive picture by involving a Jahn-Teller-type effect that is sensitive to the tensor-force-driven shell evolution. The closed subshell nucleus ^{42}Si is a particularly good example of how the tensor-force-driven Jahn-Teller mechanism leads to a strong oblate rather than a spherical shape.

DOI: 10.1103/PhysRevC.86.051301 PACS number(s): 21.60.Cs, 27.40.+z, 21.10.Pc, 21.30.Fe

Among the new frontiers in nuclear physics, one of the most important is the evolution of single-particle energies (SPEs) in nuclei far from stability, which leads to significant variation in the shell structure and even dramatic changes in the location of magic numbers [1,2]. One of the ingredients is the tensor force, which can change spin-orbit splitting significantly and leads to tensor-force-driven shell evolution [3,4]. Although many experimental examples, e.g., Refs. [5–8], have been accumulated on this phenomenon, its direct test including the fragmentation of single-particle strength has not been presented. In this Rapid Communication, we will show a test for this kind of proton $0d_{5/2}$-$0d_{3/2}$ splitting in ^{48}Ca by comparing to spectroscopic factors measured in the $(e,e'p)$ experiment [9].

We then show[1] that tensor-driven shell evolution plays a critical role in the rapid shape transition, including triaxial and γ-unstable shapes, as a function of neutron and/or proton number. In particular, we show for the first time how this shape transition at low energies can be related to the Jahn-Teller-type effect [11,12] where a geometric distortion is brought about by a particular coherent superposition of relevant single-particle states enhanced due to their (near) degeneracy.

These studies are performed, in terms of the shell model, in a unified way with a new Hamiltonian. We show calculated energy levels and $B(E2)$ values for the Si and S isotopes that are in good agreement with the experiments [13–19], and new predictions are made. Potential-energy surfaces (PESs) are shown. The PESs change rapidly as a function of neutron number and are different for Si and S. The PES for ^{42}Si shows a strong oblate shape (rather than spherical) due to the tensor-force-driven shell evolution. These PES results are interpreted in an intuitive picture which involves shell gaps and the Jahn-Teller-type effect. Two-neutron separation energies are also discussed.

We outline the present shell-model calculations. The sd and pf shells are taken as the valence shell with protons in sd and neutrons in pf. The interactions within each of these shells are based on existing interactions: USD [20] (GXPF1B [21][2]) for the sd (pf) shell, except for the monopole interactions [4,23] $V^{T=0,1}_{0d_{3/2},0d_{5/2}}$ based on SDPF-M [24] due to a problem in USD as pointed out in Ref. [2]. The monopole- and quadrupole-pairing matrix elements $\langle 0f_{7/2}0f_{7/2}|V|0f_{7/2}0f_{7/2}\rangle_{J=0,2}$ are replaced with those of KB3 [23]. This is mainly for a better description of nuclei of $N \sim 22$. Although this replacement is not so relevant to the present study where N is larger in most cases, it has been made so that the applicability of the new Hamiltonian becomes wider. The cross-shell part, most essential for the exotic nuclei discussed in this Rapid Communication but rather undetermined so far, is given basically by $V_{\rm MU}$ of Ref. [4] with the small refinements stated below. The tensor-force component is taken exactly from $V_{\rm MU}$, which implies the $\pi + \rho$ meson exchange force. It has been used in many cases [3,4], and it has been accounted for microscopically under the new concept of renormalization persistency [25] where modern realistic effective interactions are analyzed in

[1]A brief account with selected results from this Rapid Communication was presented in Ref. [10].

[2]The GXPF1B Hamiltonian was created from the GXPF1A Hamiltonian [22] by changing five $T = 1$ matrix elements and the SPE which involved $1p_{1/2}$. Such differences present no notable changes to the present result due to the minor relevance of $1p_{1/2}$.

terms of the spin-tensor decomposition technique [26–28]. The central-force component of the $V_{\rm MU}$ interaction has been determined in Ref. [4] so as to reproduce monopole properties of shell-model interactions SDPF-M (sd-shell part) and GXPF1A [22,29] by a simple Gaussian interaction. Here, we introduce a slight fine-tuning with density dependence similar to the one in Ref. [27] for its monopole part to become closer to that of GXPF1B. We include the two-body spin-orbit force of the M3Y interaction [30]. (For the present study, all these refinements produce minor changes and do not change the overall conclusions. The refinements have been made so that the new Hamiltonian works well in a wide variety of nuclei other than those of this study.) By following USD and GXPF1B, all two-body matrix elements are scaled by $A^{-0.3}$. The single-particle energies (SPEs) of the sd shell are taken from USD, and those of the pf shell are determined by requesting their effective SPEs on top of the ^{40}Ca closed shell equal to the SPEs of GXPF1B.

The Hamiltonian, hereafter referred to as SDPF-MU, is, thus, fixed prior to the shell-model calculations presented in this Rapid Communication. The diagonalization is performed by the MSHELL64 code [31]. The $V_{\rm MU}$ interaction has also been used to construct the cross-shell part of a recent shell-model Hamiltonian for p-sd shell nuclei that include neutron-rich exotic ones, which provide a good description of very light (B,C,N,O) nuclei [32].

We begin with the distribution of single-particle strength of proton sd-shell orbits. Spectroscopic factors obtained for ^{48}Ca with the $(e, e'p)$ reaction are displayed in the upper panels of Fig. 1 [9]. The $0d_{5/2}$ single-particle strength is highly fragmented due to its high excitation energy (3–8-MeV range). The spectroscopic factors obtained by the present calculation are shown in the lower left-hand panel of Fig. 1 where an overall quenching factor of 0.7 is used, which follows the standard recipe to incorporate various effects of components outside the valence shell [33]. The agreement is excellent both in the position of the peaks and in their magnitudes. However, this agreement is lost if the tensor force is removed from the cross-shell interaction as shown in the right lower panel of Fig. 1. For instance, the largest $0d_{3/2}$ and $1s_{1/2}$ peaks are in the wrong order, and the strongest peaks of $0d_{5/2}$ move towards higher energies. The $0d_{3/2}$-$0d_{5/2}$ gap of ^{48}Ca turns out to be $\sim$5 MeV in the present calculation but becomes $\sim$2 MeV larger if the cross-shell tensor force is switched off.

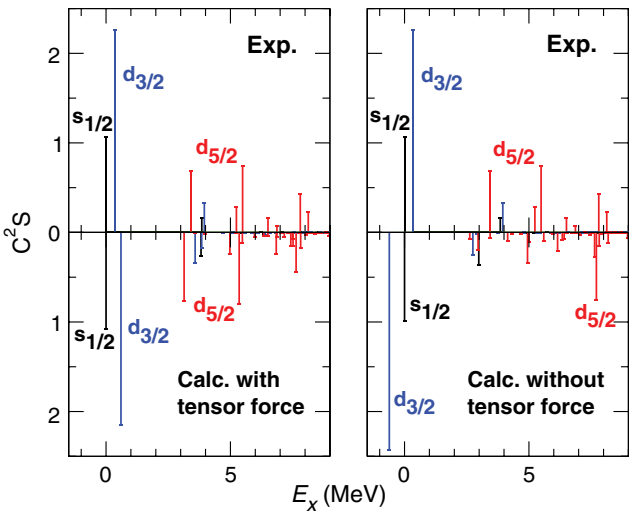

FIG. 1. (Color online) Spectroscopic factors of proton-hole states measured by ^{48}Ca$(e, e'p)$ [9] (upper) and its theoretical calculation (lower left). The cross-shell tensor force is removed in the lower right panel. The black, blue, and red bars correspond to $1s_{1/2}$, $0d_{3/2}$, and $0d_{5/2}$ states, respectively.

For ^{40}Ca, although no experimental data for the $(e, e'p)$ reaction is available [34], Bastin *et al.* suggested a reduction in the proton $0d_{5/2}$-$0d_{3/2}$ gap by 1.9 MeV from ^{40}Ca to ^{48}Ca based on reaction data [16]. Effective SPEs obtained from the SDPF-MU Hamiltonian are consistent with this and other experimental data [1]. On the other hand, the gap remains almost unchanged between ^{40}Ca and ^{48}Ca if the cross-shell tensor force is removed. We note that the spectroscopic-factor distributions for $0d_{3/2}$ and $1s_{1/2}$ also were calculated with a Green's function method by Barbieri [33], but there was no previous report on the $0d_{5/2}$ strength.

The proton-shell structure, thus, evolves from ^{40}Ca to ^{48}Ca. Because only the tensor force can change the $0d_{3/2}$-$0d_{5/2}$ gap by this order of magnitude ($\sim$2 MeV), the agreement shown in Fig. 1 provides us with the evidence from electron-scattering experiments for the tensor-force-driven shell evolution induced by the mechanism of Otsuka *et al.* [3]. This agreement also implies the validity of the present SDPF-MU Hamiltonian, especially the interaction between the proton sd and the neutron pf shells.

We now move to the shape transitions in exotic Si ($Z = 14$) and S ($Z = 16$) isotopes with even $N = 22$–28. Before discussing quantitative results, in Fig. 2, we present an intuitive picture on the relation between the shell structure and the shape of Si nuclei. To begin with, we consider only two orbits $0d_{5/2}$ and $1s_{1/2}$ of protons for the sake of simplicity. In a conventional view, $Z = 14$ is a submagic number: no mixing between $1s_{1/2}$ and $0d_{5/2}$ due to a large $1s_{1/2}$-$0d_{5/2}$ gap and/or a weak mixing force. Six protons occupy all states of $0d_{5/2}$, forming a closed subshell as depicted in Fig. 2(a). This should end up with a spherical shape for a doubly magic nucleus ^{42}Si ($N = 28$) similar to ^{34}Si ($N = 20$).

Figure 2(b) indicates another situation where sizable mixing occurs between the $1s_{1/2}$ and the $0d_{5/2}$ orbits in the case where the proton-neutron correlation is stronger than in Fig. 2(a) and competes with $1s_{1/2}$-$0d_{5/2}$ spacing. The proton-neutron interaction, apart from its monopole part, can be modeled by a quadrupole-quadrupole interaction to a good extent. Effects of this interaction can be discussed in terms of intrinsic states due to a quadrupole deformation. By assuming an axially symmetric deformation, single-particle states of the same magnetic quantum numbers, denoted as m, are mixed in the intrinsic states. Figure 2(b) shows that this occurs for $m = \pm 1/2$ between $1s_{1/2}$ and $0d_{5/2}$, with amplitudes $\sin\theta$ and $\cos\theta$, respectively. The phase of the mixing amplitude depends on the shape, prolate or oblate. In the case of Si isotopes, protons occupy the states of $m = \pm 5/2, \pm 3/2$, which yield, in total, a negative intrinsic quadrupole moment (oblate). The total intrinsic quadrupole moment gains a

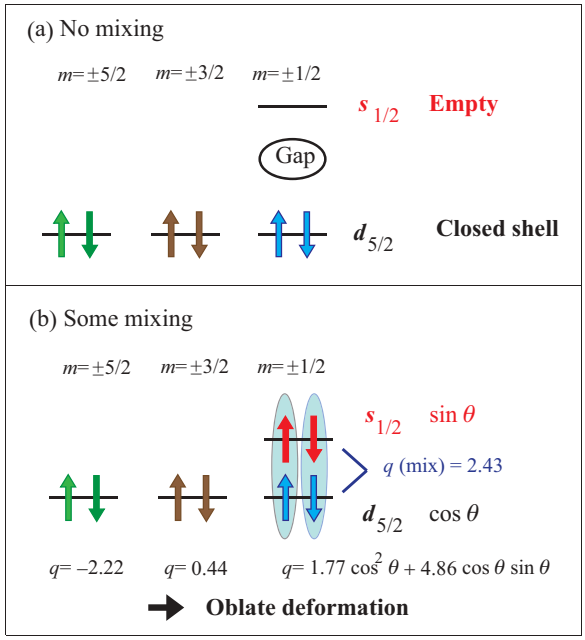

FIG. 2. (Color online) Intuitive illustration of the structure of the intrinsic state at $Z = 14$. Single-particle states of magnetic quantum numbers, denoted as m, are shown. q implies the intrinsic quadrupole moment (fm^2) obtained with harmonic oscillator $\hbar\omega = 11.8$ MeV.

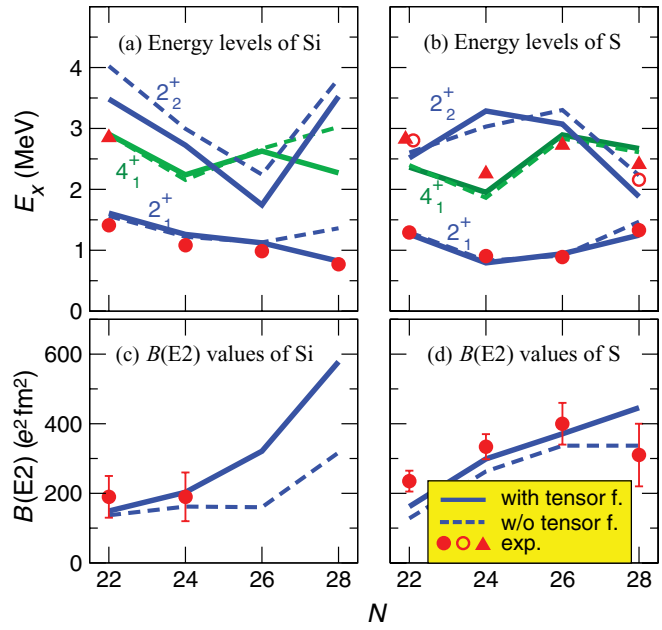

FIG. 3. (Color online) (a) and (b) $2^+_{1,2}$ (blue lines and red circles) and 4^+_1 (green lines and red triangles) energy levels and (c) and (d) $B(E2; 0^+_1 \to 2^+_1)$ values of Si and S isotopes for $N = 22$–28. Symbols are experimental data [13–19]. Solid (dashed) lines are calculations with (without) the cross-shell tensor force.

larger magnitude if the $1s_{1/2}$-$0d_{5/2}$ mixing gives a negative moment. The contribution from the proton-neutron multipole interaction to the energy of total intrinsic state is approximately proportional to the product of the proton intrinsic quadrupole moment and the neutron one. Because a similar situation can occur for neutrons in $1p_{3/2}$ and $0f_{7/2}$ with a negative intrinsic moment produced mainly by the $m = \pm 7/2$ component of $0f_{7/2}$, a stronger binding is obtained for the total intrinsic state with an oblate shape. Although the proton $0d_{3/2}$ orbit is mixed to some extent in the actual shell-model calculation, the above mechanism still holds: The occupation of $m = \pm 5/2$ remains with a large negative quadrupole moment (oblate), and the mixing can occur among $0d_{5/2}$, $0d_{3/2}$, and $1s_{1/2}$ orbits in the relevant $m = \pm 1/2$ and $\pm 3/2$ components in favor of the oblate shape.

This mechanism is of Jahn-Teller type, and it works if the mixing due to the proton-neutron correlation can compete with SPE spacings. The above intuitive pictures with Figs. 2(a) and 2(b) suggest rather robustly that the shape of ^{42}Si can be spherical or oblate but not prolate. The $0d_{5/2}$-$1s_{1/2}$ spacing is 7.8 MeV for ^{42}Si with the SDPF-MU Hamiltonian in the filling scheme. This is, indeed, comparable with the ground-state expectation value -13.2 MeV of the multipole proton-neutron interaction, obtained by the shell-model calculation discussed below. Regarding the tensor force, when many neutrons occupy the $0f_{7/2}$ orbital, the proton $0d_{5/2}$ is raised due to the mechanism of Otsuka *et al.* [3], discussed for the $(e, e'p)$ data above. This effect is included in the result of the SDPF-MU Hamiltonian by reducing $0d_{5/2}$-$1s_{1/2}$ spacing by 1.1 MeV for ^{42}Si. We see its importance now.

Here, we quantitatively investigate the structure of Si and S isotopes in the context of the shell-model calculations with the SDPF-MU Hamiltonian. Figure 3 exhibits properties of even-A Si and S isotopes. Effective charges are $(e_p, e_n) = (1.35e, 0.35e)$ where an isoscalar shift, fixed for lighter isotopes, is taken. The overall agreement with the experiment is excellent in Fig. 3. For instance, in the present result, 2^+_1 levels of Si isotopes keep coming down as N increases consistently with the experiment. The nice agreement suggests that the intuitive picture in Fig. 2(b) works particularly well towards ^{42}Si, which results in a strongly deformed shape with low excitation energies consistent with the recent measurements in GANIL [16]. However, if the tensor force is omitted from the cross-shell interaction, the 2^+_1 level of ^{42}Si goes up, which suggests the case in Fig. 2(a). Figure 3 exhibits results for S isotopes also in good overall agreement including a bumpy behavior of the 4^+_1 level. Earlier shell-model calculations with empirical interactions [35,36] give larger deviations and/or different trends from the experiments. In Ref. [35], different Hamiltonians are taken between $Z \leqslant 14$ and $Z \geqslant 15$ isotopes related to the monopole pairing strength in the pf shell. The deviation from the experiment becomes larger if this change is switched off. The present Hamiltonian is the same for all isotopes and has been fixed prior to the shell-model calculations so as to make predictions.

The PES can be used to understand shapes contained in theoretical calculations. Figures 4 and 5 exhibit PESs for Si and S isotopes, respectively, obtained by the constrained Hartree-Fock method [37] for the SDPF-MU Hamiltonian. The full Hamiltonian is taken in panels (a)–(d) of the two figures, whereas, the cross-shell tensor force is removed in panels (e)–(h). We begin with PESs of Si isotopes (Fig. 4). Shape evolutions are clearly seen in both sequences (a)–(d)

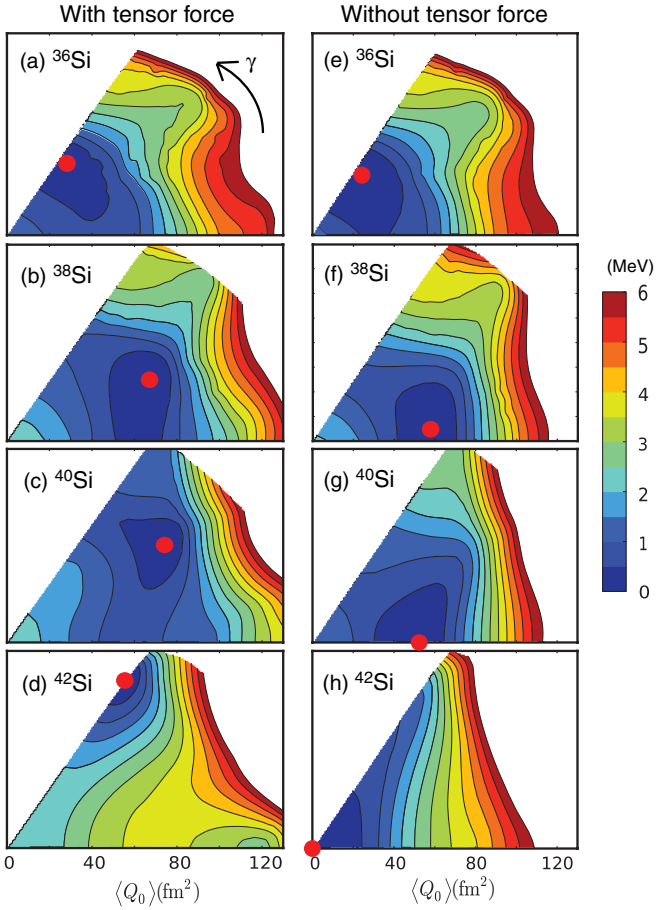

FIG. 4. (Color online) Potential-energy surfaces of Si isotopes for $\gamma = 0 \sim 60^\circ$ from $N = 22$ to 28 calculated with (left) and without (right) the cross-shell tensor force. The energy minima are indicated by red circles.

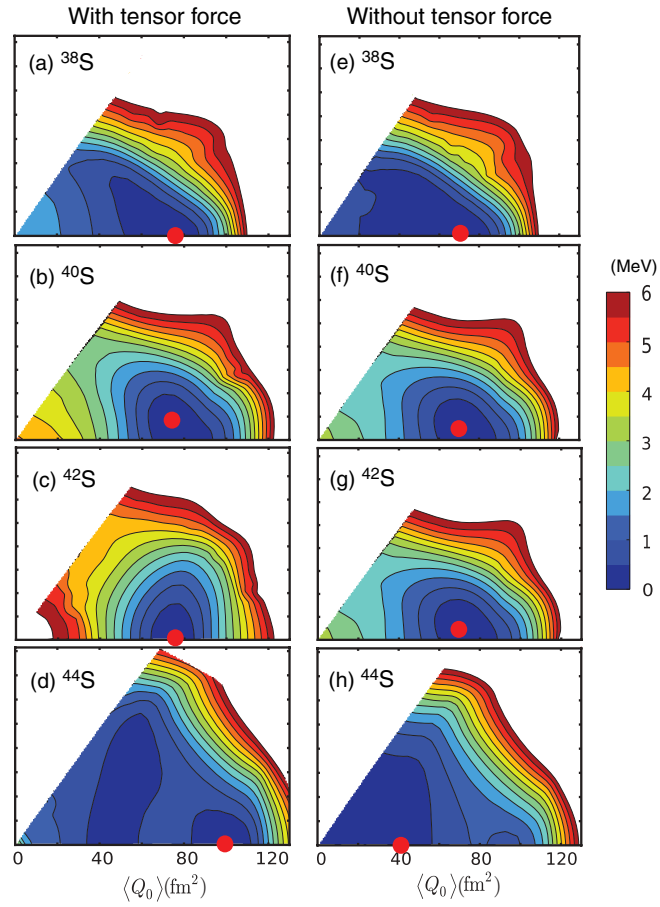

FIG. 5. (Color online) Potential-energy surfaces of S isotopes from $N = 22$ to 28. See the caption of Fig. 4.

and (e)–(h), which start with similar patterns in ^{36}Si. The shape evolves as more neutrons occupy the pf shell with distinct differences between the two sequences. In (b) and (c), the deformation becomes stronger from (a) with triaxial minima, whereas, the shape becomes more modestly prolatelike in (f) and (g). In (d), one finds a strongly oblate shape with a sharp minimum, but the minimum is at the spherical shape in (h). This strong oblate deformation produces a low 2^+ level and a large $B(E2)$ in Fig. 3 for the "doubly closed" ^{42}Si. Thus, the shape of exotic Si isotopes changes significantly within the range of $\Delta N \sim 6$. This feature is partly due to growing collectivity with more neutrons in the pf shell but is also a manifestation of the Jahn-Teller-type effect driven by the tensor force. Without the tensor force, the SPE spacings are too large, and the correlation energies cannot produce this effect.

The γ-unstable deformation is well developed in Fig. 4(c), and this can be confirmed by the low-lying 2_2^+ level of ^{40}Si in Fig. 3. This level seems to agree with a recent γ-ray experiment [15] where either of γ rays 638(8) and 845(6) keV appears to directly feed the 2_1^+ state. We stress that the 2_2^+ level is sensitive to the tensor force through γ instability in Si isotopes. In fact, the ratio $E_x(2_2^+)/E_x(2_1^+)$ is as low as 1.5 for ^{40}Si, whereas, it becomes 4.4 for ^{42}Si. The former is a prominent signature of γ instability, whereas, the latter is consistent with a vibration from a profound PES minimum of axially symmetric deformation. Thus, the change from ^{40}Si to ^{42}Si is an intriguing example of the rapid and unexpected structure evolution. If the tensor force is switched off in the cross-shell interaction, $E_x(2_1^+)$ of ^{42}Si is raised, but the $B(E2)$ value is still larger than that of ^{40}Si. This is partly due to the stretched minimum in Fig. 4(h) and is partly due to relatively enhanced proton contribution in the $E2$ transition because of the $N = 28$ closure.

The situation is quite different with the PESs of S isotopes (Fig. 5). With two more protons added to the Si isotopes, the occupancy of the $0d_{5/2}$ orbit is closer to that of a closed shell. The mixing between $1s_{1/2}$ and $0d_{3/2}$ then plays a decisive role, which leads to a structure that favors prolate deformation. As for neutrons, $m = \pm 7/2$ components of $0f_{7/2}$ carry large negative intrinsic quadrupole moments and are crucial for the oblate shape, whereas, the others have positive or small negative values. In S isotopes, as protons favor prolate shapes, the neutron sector becomes prolate for $N < 28$ by keeping the $m = \pm 7/2$ states (almost) unoccupied. At $N = 28$, the $m = \pm 7/2$ states are occupied more. However, the neutron $0f_{7/2}$-$1p_{3/2}$ spacing decreases from Ca isotopes to Si and S ones due to the vacancy of proton $0d_{3/2}$, and the excitation from

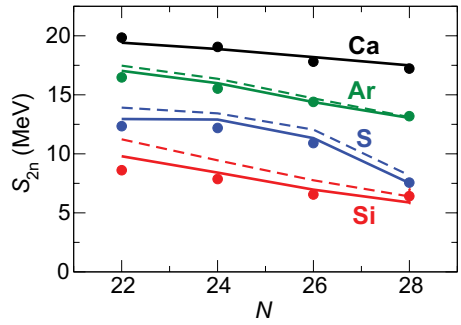

FIG. 6. (Color online) Two-neutron separation energies of Si and S isotopes from $N = 22$ to 28. Solid (dashed) lines are calculations with (without) the cross-shell tensor force. Points are experimental data [40,41].

the $m = \pm 7/2$ states to other orbits does not cost much energy as compared to gains from proton-neutron correlation. This gives rise not to an oblate minimum, but to a triaxial softness. Thus, the shape is determined, in the present cases, primarily by the proton sector. We would like to emphasize the crucial role of protons in determining the shapes of Si and S isotopes. We comment that the quasi-SU(3) scheme [38], constructed for the configurations composed of almost degenerate j and $j - 2$ orbits only, e.g., $0f_{7/2}$ and $1p_{3/2}$, favors an oblate shape at $N = 28$.

Panels (d) and (h) in Fig. 5 show prolate minima with opposite trends from panels (c) and (g), which are rather similar to each other. This difference arises within prolate shapes with shallow minima, and thereby, its appearance in the energy levels is modest (see Fig. 3). The difference in the shapes between Si and S isotopes may suppress transfer reactions, for instance, two-proton removal from ^{44}S [39].

We now discuss the two-neutron separation energies (S_{2n}) shown in Fig. 6. The agreement between the experiment and the full calculation is quite good within $\sim$0.5 MeV, except for the $N = 22$ Si value with a discrepancy of 1.2 MeV due to the mixing of intruder configurations in ^{34}Si, an issue outside this Rapid Communication. If the tensor force is switched off, deviations of 1–3 MeV occur for Si and S isotopes in the direction of larger S_{2n} values. This means that the tensor-force effect is repulsive and becomes larger from Ca to Si isotopes as a whole, consistent with the tensor-force-driven shell evolution. This evolution induces stronger deformation in some cases, e.g., ^{42}Si where additional binding energy is gained and can partly cancel this repulsive effect.

Although Si and S isotopes have been discussed with density-functional methods, which include the appearance of oblate shapes [42–45], there are problems to be solved. No systematic calculations have been reported for levels and $B(E2)$'s of Si isotopes. The 2_1^+ level calculated in Ref. [45] reproduces the experiment for ^{44}S but deviates by a factor of 2 for ^{42}Si. Figures 3(a) and 3(b) show that the 2_1^+ level of ^{42}Si is sensitive to the tensor force, whereas, that of ^{44}S is not. The difference between ^{42}Si and ^{44}S in Ref. [45] might be relevant to this. The systematics of the 2_1^+ level in S isotopes shows an opposite trend in Ref. [44]. It will also be of interest to see single-particle properties given by these papers. For instance, the proton $0d_{5/2}$-$0d_{3/2}$ gap remains almost unchanged from ^{40}Ca to ^{48}Ca in these calculations, but this contradicts the trend seen in the $(e, e'p)$ data [9].

To summarize, we have discussed the tensor-force-driven reduction in the spin-orbit splitting by the mechanism of Otsuka *et al.* [3], for the first time, in terms of distribution of spectroscopic factors measured by the ^{48}Ca$(e, e'p)$ experiment [9]. The SDPF-MU Hamiltonian has been introduced based on the $V_{\rm MU}$ interaction. The spectroscopic-strength distribution provides a stringent test of this Hamiltonian. The levels, $B(E2)$'s, and S_{2n} of exotic Si and S isotopes are described by the same Hamiltonian in good agreement with all known experiments, which exhibit a rather rapid change, as a function of N, for Si isotopes but a quite different change for S isotopes. The tensor-force-driven shell evolution [3] plays a crucial role in those shape transitions through the Jahn-Teller-type effect, including a robust mechanism that favors stable oblate shapes at subshell closures, such as ^{42}Si. The $B(E2)$ values are sensitive to the tensor force. The next region of the nuclear chart where such oblate shapes may occur is near ^{78}Ni.

This work was, in part, supported by a MEXT Grant-in-Aid for Scientific Research Grant No. (A) 20244022 and for Young Scientists Grant No. (B) (21740204) and NSF Grant No. PHY-1068217. This work is a part of the CNS-RIKEN joint research project on large-scale nuclear-structure calculations.

[1] A. Gade and T. Glasmacher, Prog. Part. Nucl. Phys. **60**, 161 (2008); O. Sorlin and M.-G. Porquet, *ibid.* **61**, 602 (2008).
[2] T. Otsuka *et al.*, Phys. Rev. Lett. **87**, 082502 (2001).
[3] T. Otsuka, T. Suzuki, R. Fujimoto, H. Grawe, and Y. Akaishi, Phys. Rev. Lett. **95**, 232502 (2005).
[4] T. Otsuka, T. Suzuki, M. Honma, Y. Utsuno, N. Tsunoda, K. Tsukiyama, and M. Hjorth-Jensen, Phys. Rev. Lett. **104**, 012501 (2010).
[5] J. P. Schiffer *et al.*, Phys. Rev. Lett. **92**, 162501 (2004).
[6] L. Gaudefroy *et al.*, Phys. Rev. Lett. **97**, 092501 (2006).
[7] K. T. Flanagan *et al.*, Phys. Rev. Lett. **103**, 142501 (2009).
[8] I. G. Darby *et al.*, Phys. Rev. Lett. **105**, 162502 (2010).
[9] G. J. Kramer *et al.*, Nucl. Phys. A **679**, 267 (2001).
[10] T. Otsuka *et al.*, Nucl. Phys. A **805**, 127c (2008).
[11] H. A. Jahn and E. Teller, Proc. R. Soc. London, Ser. A **161**, 220 (1937).
[12] P.-G. Reinhard and E. W. Otten, Nucl. Phys. A **420**, 173 (1984).
[13] Evaluated Nuclear Structure Data File (ENSDF), http://www.nndc.bnl.gov/ensdf/.
[14] X. Liang *et al.*, Phys. Rev. C **74**, 014311 (2006).
[15] C. M. Campbell *et al.*, Phys. Rev. Lett. **97**, 112501 (2006).
[16] B. Bastin *et al.*, Phys. Rev. Lett. **99**, 022503 (2007).
[17] Z. M. Wang *et al.*, Phys. Rev. C **81**, 054305 (2010).
[18] D. Sohler *et al.*, Phys. Rev. C **66**, 054302 (2002).
[19] D. Santiago-Gonzalez *et al.*, Phys. Rev. C **83**, 061305(R) (2011).
[20] B. A. Brown and B. H. Wildenthal, Annu. Rev. Nucl. Part. Sci. **38**, 29 (1988).

[21] M. Honma *et al.*, RIKEN Accelerator Progress Report **41**, 32 (2008).
[22] M. Honma *et al.*, Eur. Phys. J. A **25**, 499 (2005).
[23] A. Poves and A. Zuker, Phys. Rep. **70**, 235 (1981).
[24] Y. Utsuno, T. Otsuka, T. Mizusaki, and M. Honma, Phys. Rev. C **60**, 054315 (1999).
[25] N. Tsunoda, T. Otsuka, K. Tsukiyama, and M. Hjorth-Jensen, Phys. Rev. C **84**, 044322 (2011).
[26] M. W. Kirson, Phys. Lett. B **47**, 110 (1973).
[27] B. A. Brown, W. A. Richter, R. E. Julies, and B. H. Wildenthal, Ann. Phys. **182**, 191 (1988).
[28] N. A. Smirnova *et al.*, Phys. Lett. B **686**, 109 (2010).
[29] M. Honma, T. Otsuka, B. A. Brown, and T. Mizusaki, Phys. Rev. C **69**, 034335 (2004).
[30] G. Bertsch *et al.*, Nucl. Phys. A **284**, 399 (1977).
[31] T. Mizusaki, N. Shimizu, Y. Utsuno, and M. Honma, MSHELL64 code (unpublished).
[32] C. Yuan, T. Suzuki, T. Otsuka, F. Xu, and N. Tsunoda, Phys. Rev. C **85**, 064324 (2012).
[33] C. Barbieri, Phys. Rev. Lett. **103**, 202502 (2009).
[34] G. J. Kramer *et al.*, Phys. Lett. B **227**, 199 (1989).
[35] F. Nowacki and A. Poves, Phys. Rev. C **79**, 014310 (2009).
[36] K. Kaneko, Y. Sun, T. Mizusaki, and M. Hasegawa, Phys. Rev. C **83**, 014320 (2011).
[37] T. Mizusaki, T. Otsuka, Y. Utsuno, M. Honma, and T. Sebe, Phys. Rev. C **59**, R1846 (1999).
[38] A. P. Zuker, J. Retamosa, A. Poves, and E. Caurier, Phys. Rev. C **52**, R1741 (1995).
[39] J. Fridmann *et al.*, Nature (London) **435**, 922 (2005).
[40] G. Audi, A. H. Wapstra, and C. Thibault, Nucl. Phys. A **729**, 337 (2003).
[41] B. Jurado *et al.*, Phys. Lett. B **649**, 43 (2007).
[42] G. A. Lalazissis, D. Vretenar, P. Ring, M. Stoitsov, and L. M. Robledo, Phys. Rev. C **60**, 014310 (1999).
[43] S. Peru *et al.*, Eur. Phys. J. A **9**, 35 (2000).
[44] R. Rodríguez-Guzmán, J. L. Egido, and L. M. Robledo, Phys. Rev. C **65**, 024304 (2002).
[45] Z. P. Li, J. M. Yao, D. Vretenar, T. Nikšić, H. Chen, and J. Meng, Phys. Rev. C **84**, 054304 (2011); Z. Li *et al.*, *ibid.* **84**, 112501 (2005).